Hyperfine interactions in cluster models of the P_b defect center

Michael Cook and C. T. White
Naval Research Laboratory (Code 6119), Washington, D.C. 20375-5000
(Received 20 May 1988)

Hyperfine interactions in the P_b center (denoted schematically as $Si_3 \equiv Si\cdot$) at the Si(111)/SiO_2 interface have been studied with use of spin-polarized self-consistent multiple-scattering $X\alpha$ calculations on $Si_{22}H_{21}/Si_6O_{18}H_6$ and $Si_{22}H_{27}$ cluster models. Our theoretical hyperfine tensor agrees very well with experiment when the trivalent atom Si' is relaxed by a value typical of geometries found for the neutral paramagnetic charge state in semiempirical and *ab initio* cluster calculations. Spin-polarization effects are found to be very important for a detailed description of the P_b defect, particularly with respect to the hyperfine couplings at nuclei close to the defect atom. The largest such superhyperfine interaction is produced not by the nearest-neighbor atoms as has commonly been assumed, but by three second-nearest neighbors located below Si' in the bulk *c*-Si. The isotropic and anisotropic superhyperfine components and the direction of the principal axes predicted by the present calculations have been confirmed by recent ESR experiments.

I. INTRODUCTION

The performance of metal-oxide-semiconductor (MOS) devices is degraded by electrically active defects produced in processing or by exposure to ionizing radiation or high-electric-field stress.[1,2] Among the most important and most thoroughly studied of these is the P_b center (denoted schematically as $Si_3 \equiv Si\cdot$), a trivalent-silicon defect located at the Si/SiO_2 interface. The P_b center is amphoteric, with three accessible oxidation levels: the neutral paramagnetic state, and two charged diamagnetic states obtained by trapping an electron or a hole at the unsatisfied Si bond. P_b has recently been shown to be responsible for most of the fast surface states (N_{st}) at the semiconductor-oxide interface.[3-5]

Si/SiO_2 interface traps such as the P_b center and related dangling-bond defects (e.g., the E_1' center, $O_3 \equiv Si\cdot$) have been studied intensively by a wide range of experimental techniques including *C-V* measurements,[3,4,6] avalanche injection of electrons or holes,[7,8] deep-level transient spectroscopy (DLTS),[9,10] spin-dependent thermal emission,[9] photoconductive resonance,[11] and photothermal deflection.[12,13] The most diagnostically useful information about the nature and structure of these defects has come from the *g* tensors and hyperfine interactions measured by ESR experiments.[14-20] Dangling-bond defects typically occupy one-electron states situated deep in the band gap between the highest-energy bonding levels (top of the valence band) and the lowest-energy antibonding levels (bottom of the conduction band). They are consequently well localized in space; the defect wave function resembles a small-molecule orbital embedded in and interacting with an extended host matrix. The *g* tensors and hyperfine tensors of such defects are sensitive probes of the bonding and spin-density distribution in the neighborhood of the unpaired electron. The specific, detailed information they provide about the local environment of paramagnetic centers is essential in characterizing defect structure, including the degree of localization, orientations with respect to host crystal axes, and identification of near-neighbor atoms, bond relaxations, and reconstructions.

Although sophisticated modern magnetic resonance techniques are being applied to Si/SiO_2 defects, most theoretical analyses of the experimental results have been conducted at a very simplified level. The most widely applied interpretative tool is the localized hybrid-orbital picture.[18,21,22] The assumptions and approximations of this picture are effectively identical to those of ligand-field theory (LFT),[23-25] with the dangling hybrid assuming the role played by nonbonding metal *d* orbitals in LFT. This picture has been very successful for characterizing the gross features of defects, e.g., for associating the principal axes of *g* tensors and hyperfine tensors with local coordinate axes and identifying large changes in local bond angles (rehybridizations) at the defect atom.[26] But for quantitative work, particularly when weak superhyper- fine interactions are involved, there are a number of reasons why more sophisticated approaches should be used.

First, the local-hybrid model ignores spin-polarization effects by assuming that the net spin density in the system is identical to the charge density of the singly occupied defect orbital. Spin polarization can be very important: for example, it is entirely responsible for the existence of nonzero isotropic proton hyperfine coupling constants in organic π radicals, which can be as large as ~ 20 G. Intra-atomic spin polarizations can be as significant as interatomic effects. The polarization of atomic cores by spin density in the valence levels plays a major role in determining the net hyperfine interaction at nuclei of the heavier atoms. An equally serious approximation is that the shapes of the atomic *s*- and *p*-valence orbitals [as measured by their values of $|\psi_s(0)|^2$ and $\langle r^{-3}\rangle_p$] are considered to be unperturbed by the host environment so that values taken directly from atomic Hartree-Fock wave functions can be used. In fact, both quantities can be significantly perturbed by valence interactions.[27] As

commonly used, the local-hybrid model also neglects the possibility of contributions to the anisotropic hyperfine tensor involving *d*-orbital populations on silicon or spin density located on neighboring atoms. At its best, the localized hybrid–AO picture (where AO is atomic orbital) is interpretative rather than predictive. When there is more than one likely source of a given interaction, the model is unable to distinguish among the possibilities on the basis of first principles. It is also subject to the usual uncertainties of least-squares fitting, so that it becomes a less useful tool as spectra become more complicated or broadened, and in cases where weak splittings and shoulders due to superhyperfine interactions with more distant nuclei are important.

More sophisticated, predictive theoretical approaches to dangling-bond defects have proceeded along several routes. In the solid-state community, localized defects have been treated by Green's functions using the tight-binding model[28–30] or density functionals;[31] the defect is embedded in a Bethe lattice[29,30] or supercell[31] host. Fowler *et al.*[32–35] have carried out studies of cluster models for defect centers using the classic self-consistent semiempirical methods of quantum chemistry [e.g., MINDO/3 (Bingham-Dewar-Lo modified intermediate neglect of differential overlap method),[36] MOPN (the open-shell version of MINDO/3),[37] and MNDO (Dewar-Thiel modified neglect of diatomic overlap method)[38]]. A limited number of *ab initio* cluster studies have also been done.[39,40] This work has concentrated heavily on questions such as reconstructions of bonds in the vicinity of the defect atom, but has given little attention to the ESR data themselves. In a system containing atoms no heavier than Si it is possible in principle to calculate the hyperfine tensors directly from the ground-state wave function. But in practice, none of the methods above is well suited to such calculations. Green's function and other solid-state methods typically ignore all spin-polarization effects. MOPN does account for spin polarization within the valence shells. However, the matrix elements required for calculating hyperfine interactions are not determined in the parametrization of the method; and because the atomic basis set is not explicit, the necessary integrals cannot be calculated directly. This makes it necessary to introduce additional parameters or to appeal to isolated-atom integrals in order to correlate theoretical spin populations with experimental hyperfine couplings.[37] *Ab initio* methods can certainly be used to compute hyperfine tensors, but it is expensive and time consuming to compute large Si clusters in spin-unrestricted *ab initio* formalisms so that one is forced to use small atomic bases or effective core potentials which severely restrict the ability of the wave function to respond to spin-polarization effects.

In this paper we report and discuss hyperfine tensor results from a set of self-consistent, spin-polarized multiple-scattering (MS) $X\alpha$ calculations on finite-cluster models representing the P_b defect at the Si(111)/SiO_2 interface. The MS Slater-Johnson $X\alpha$ method[41–43] is particularly appropriate for such a study. It is very rapid computationally, so that large model clusters can be examined: there have been a number of previous applications of the MS $X\alpha$ method to large Si-rich systems.[44–50] The spatial form of each MS $X\alpha$ radial function is found by explicit numerical integration of the one-electron Schrödinger equation in the self-consistent potential of its atomic sphere. The flexibility of these functions allows the atomic basis to respond sensitively to radial polarization effects, which often make a comparatively small contribution to the total energy but have a large effect on the hyperfine couplings. Unlike Hartree-Fock methods, density-functional methods such as MS $X\alpha$ satisfy Fermi statistics for fractional as well as integral occupation numbers.[41] This gives a smooth, consistent relationship between spin-restricted (closed-shell) and spin-polarized (open-shell) formalisms, leading to generally good accuracy in the values of properties depending on the spin density [e.g., as in recent discrete-variational-method (DVM) $X\alpha$ calculations for the isotropic proton hyperfine coupling constants in organic π radicals].[51] This consistency is particularly important in studying the P_b center, where both diamagnetic and paramagnetic charge states are of interest.

Procedures have been developed for calculating molecular properties directly from the partitioned-charge representation of the MS $X\alpha$ wave function.[27,52–54] Studies of a range of molecular properties have shown that these procedures give results of roughly double-zeta *ab initio* quality;[52,53] the most accurately calculated matrix elements are typically those which, like the integrals involved in hyperfine interactions, weight most heavily regions of space close to the nuclei where the MS $X\alpha$ muffin-tin potential approximation is least severe. In transition metals and other very heavy atoms the importance of spin-orbit interactions and the sensitivity of inner-core polarizations can cause problems in the calculation of accurate hyperfine couplings,[55,56] but no such difficulties are anticipated for atoms of the second row.

In the present paper we concentrate primarily on the analysis of hyperfine interactions in our largest P_b center cluster models. A preliminary account of some of these results has been given earlier.[57] Aspects of these calculations apart from the hyperfine interactions, including one-electron levels and interface states, the role of Si *d* orbitals, and the effects of cluster size, will be discussed in a subsequent publication. In addition to the model clusters considered explicitly in this paper, a number of smaller silicon and silica clusters have been studied in order to investigate the effects of cluster size and angular basis, and to verify that the results are not sensitive to the particular values of the sphere radii and α values which define the MS $X\alpha$ model.

In Sec. II we describe and discuss our cluster models for the P_b center. The hyperfine calculations are presented and analyzed in Sec. III. Section IV summarizes the principal conclusions.

II. MODEL CLUSTERS

The largest cluster model that we have considered for the P_b center is shown in Fig. 1. This $Si_{22}H_{21}/Si_6O_{18}H_6$ cluster contains 73 atoms and 563 electrons, and measures 14 Å across. It has C_{3v} symmetry about the *z* axis;

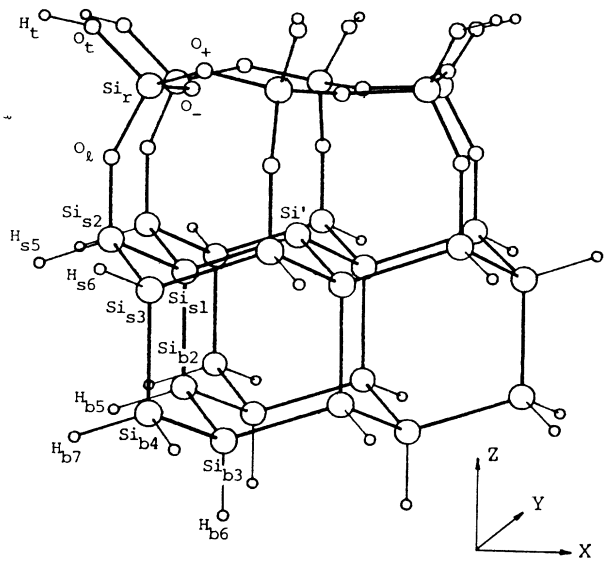

FIG. 1. Ball-and-stick model of the $Si_{22}H_{21}/Si_6O_{18}H_6$ P_b defect cluster. The sphere radii are in the same ratios as the MS $X\alpha$ radii but are greatly reduced in size for clarity. Only one atom from each symmetry-equivalent set is labeled explicitly.

the (x,z) plane is one of the three σ_v reflection planes. The largest spheres in the figure represent Si atoms. Spheres of intermediate size denote O atoms, while the smallest spheres are H-atom saturators. Bond angles and bond lengths in the model are given in Table I.

The crystalline-Si half of the cluster is a roughly hemispherical fragment of 22 Si atoms formed from three fused adamantanelike cages. It includes all lower-hemisphere neighbors of the central defect atom Si' out to a distance of 5.43 Å (fourth-nearest neighbors). The (x,y) plane forms the (111) surface of the c-Si phase. H atoms saturate the unsatisfied Si bonds at the exposed surfaces of the Si_{22} fragment and sweep them down out of the HOMO-LUMO (highest occupied molecular orbital—lowest unoccupied molecular orbital) gap into the valence bands to prevent any unphysical mixing of the defect orbital with dangling-bond surface states. These H saturators are positioned along c-Si bond directions, but the Si—H bond lengths are set equal to 1.48 Å, the experimental bond distance in silane.[59] The c-Si atoms are distinguished by subscripts s or b, denoting surface or bulk, to indicate whether the atom is in the surface monolayer or not, and by numerical subscripts which increase monotonically with distance from Si'. For example, the three Si_{s1} atoms are the defect atom's nearest neighbors in the surface monolayer: the three Si_{b2}'s are the second neighbors in the bulk, etc.

TABLE I. Geometry of the $Si_{22}H_{21}/Si_6O_{18}H_6$ cluster model.

Bond length (Å)		Bond angle (deg)	
		c-Si phase	
All Si—Si	2.352[a]	All Si—Si—Si	109.47
All Si—H	1.480[b]		
		SiO_2 phase	
All Si—O	1.610[c]	All O—Si—O	109.4–109.5
All O—H	0.957[d]	Si_r—O_-—Si_r	138.6
		Si_r—O_+—Si_r	149.3
		Si_r—O_l—Si_{s2}	150.9
		Si_r—O_t—H_t	143.5[e]

[a]Experimental c-Si value (Ref. 58).
[b]Experimental SiH_4 value (Ref. 59).
[c]From α-quartz (Ref. 60).
[d]Experimental H_2O value (Ref. 61).
[e]Si—O—Si from α-quartz (Ref. 60). The experimental distribution of Si—O—Si angles in crystal structures of silicates and silica polymorphs is primarily in the range 135°–160° (Ref. 62).

The Si_{22} c-Si fragment makes a more satisfactory model than either slightly smaller or slightly larger clusters in that every Si atom is a member of at least one six-membered ring, ensuring that two or more of its bonds are to other silicons. This represents a local minimum in the [H]/[Si] ratio as a function of fragment size. One concern in modeling a solid-state defect by a finite cluster is that the saturators at the cluster surface have a different electronegativity than the bulk atoms; the perturbation of the electronic structure due to this electronegativity difference should be reduced when the [H]/[Si] ratio is decreased. If the radius of the c-Si fragment were made slightly larger by replacing each H saturator in the present cluster by Si, then every additional silicon would have to be added as an SiH_3 group and the [H]/[Si] ratio would be increased significantly ($Si_{43}H_{63}$). The surface of the cluster would of course also be moved farther from the defect atom by expanding the cluster, but only by the length of one Si—Si bond. It is unlikely that this would improve the model enough to offset the perturbing effect of the increased [H]/[Si] ratio and justify the much greater computational expense.

The silica side of the junction is modeled by a puckered, ditrigonal ring of six SiO_4 tetrahedra. Three O_+ atoms are puckered up above the plane of six-ring silicons Si_r, and three O_- atoms are puckered slightly downwards. Six O_l—Si_{s2} linking bonds form the interface, and the silica cap is terminated by six O_t—H_t groups. This model for the silica phase has a number of attractive features. Ditrigonal rings are common in the naturally occurring phases of silica, particularly tridymites[63,64] (in β-tridymite the whole structure is of this form; see Fig. 2). Konnert, Karle, and co-workers[65,66] have found from radial distribution-function analyses of x-ray and neutron diffraction experiments that the short-range order in silica glass is more closely related to that of tridymite than of any other common SiO_2 phase. More recently, Ourmazd *et al.*[67] have argued on the basis of high resolution transmission electron microscopy that in an epitaxial Si(100)/SiO_2 interface, the silica side of the junction is effectively a crystalline tridymite. These experimental results suggest that ditrigonal six-membered rings predominate in the local structure of amorphous silica. By adjusting the dihedral angles (the puckering) of a ditrigonal ring so as to flatten it slightly, the ring can be fitted neatly onto a hexagon of Si(111) surface atoms with very little strain. The local bonding at Si_r is kept regular and tetrahedral, consistent with the nearly invariant geometry of SiO_4 tetrahedra in silicates and silica polymorphs.[64,66,68] The spread of Si—O—Si angles is

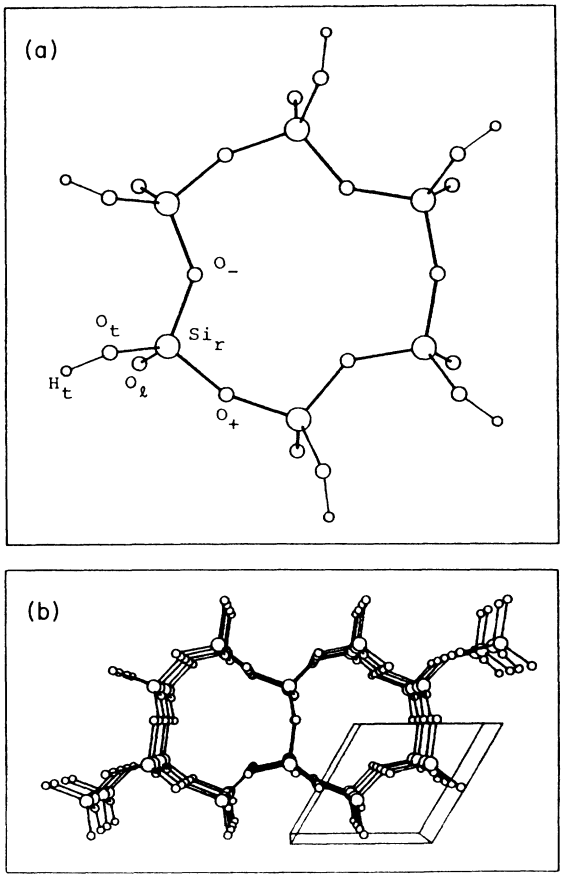

FIG. 2. (a) Top view of the $Si_6O_{18}H_6$ ring in the model of Fig. 1, showing the "boxy" shape characteristic of a ditrigonal ring. (b) Crystal structure of a hexagonal β-tridymite (coordinates from Ref. 63). The unit cell is outlined at lower right. The view is down the hexagonal axis, along channels formed by stacked ditrigonal rings.

139°–151° in our model. This is a reasonable range: In the crystal structure of a meteoritic α-tridymite with a large *Cc* unit cell, for example, Dollase and Baur[63] found all but one of the Si—O—Si angles (96%) to lie in the range 142°–159°.

Using this ring to represent the SiO_2 phase, the P_b dangling bond points into a silica microvoid. The radius of the cavity is 2.2 Å (measured from the Si′ nucleus to the van der Waals surface[69] of O_-). The surfaces of O_l and O_+ are farther away, at 2.8 and 3.0 Å, respectively. This is a sufficiently large space to allow small radical species (e.g., H) diffusing through the silica to be accommodated in a bond to Si′. Saturation by diffusing H atoms is believed to be responsible for the decrease in the number of paramagnetic P_b centers observed on thermal or hydrogen annealing,[20] so that a microvoid of this size or larger should be expected in a realistic P_b structure. The primary access to the microvoid is through a 1.4-Å-diam opening in the center of the capping silica ring, bounded by the van der Waals surfaces of the three O_- atoms (Fig. 2). This opening can presumably be widened somewhat by thermal excitation of ring vibrations. The $Si_6O_{18}H_6$ silica cap consequently provides a degree of protection for the Si′ dangling bond against saturation by the larger radical species present in silica, but, consistent with observation, it does permit an H radical to reach the defect atom and coordinate to it in a thermally activated process.

The $Si_{22}H_{21}/Si_6O_{18}H_6$ model has been made as compact as possible to minimize the effects of the MS $X\alpha$ muffin-tin potential approximations on the electronic structure. It has also been kept at high symmetry (C_{3v}) to take advantage of the reduction in computational effort due to a doubly degenerate (E) irreducible representation. Actual P_b centers might well not all be so compact or symmetrical. In particular, entropic considerations would oppose the presence of a closed, symmetrical ditrigonal ring capping each defect atom. However, experimentally the g tensor and largest hyperfine tensor of the P_b center are found to have axial symmetry around the ⟨111⟩ direction, consistent with a threefold axis normal to the interface.[18,20] Whatever the degree of disorder or asymmetry about the defect, it is sufficiently small that the concept of an average high-symmetry P_b center is still meaningful, and the symmetric model that we use should give an accurate representation of this average P_b structure.

The most important unresolved structural question concerning the P_b center is what value to use for the vertical reconstruction $\Delta z_{Si'}$ of the defect atom away from its ideal, tetrahedral *c*-Si position. Simple considerations of orbital energy variation as a function of geometry[70] (Walsh diagrams) as well as self-consistent semiempirical[34,35] and *ab initio*[39,40] calculations agree that $\Delta z_{Si'}$ should be negative in the ESR-active neutral charge state. As compared to a fourfold-coordinated silicon with tetrahedral bonding, the Si′—Si_{s1} bonds are strengthened and shortened: In local hybridization language the doubly occupied Si′ hybrids bonding to Si_{s1} increase their s character at the expense of the singly occupied nonbonding orbital, which becomes more p-like. The size of this reconstruction should affect the hyperfine interactions significantly because of the variation in s versus p character induced at Si′.

The qualitative trend of this simple local-hybrid picture is certainly correct, but the value of $\Delta z_{Si'}$ is not known accurately. Theoretically calculated values appear to be sensitive to the size of the model cluster and to the size of basis sets.[34,39,40,71] For our present purposes we consider calculations at two geometries: the unrelaxed tetrahedral geometry $\Delta z_{Si'}=0$ Å, which serves as a well-defined benchmark, and $\Delta z_{Si'}=-0.09877$ Å, a representative reconstructed value taken from a recent semiempirical total energy minimization by Edwards.[72] All other atoms are held fixed.

Three calculations will be discussed. Models holding Si′ at the tetrahedral position have been studied both with and without the SiO_2 cap in order to measure the effect of the silica phase on the properties of the P_b center. When the cap is removed, the Si_{s2} atoms are saturated by H, as for the rest of the cluster surface. One relaxed-Si′ calculation has been carried out on the uncapped cluster.

The MS $X\alpha$ sphere radii have been taken as $2.50a_0$ (Si), $1.50a_0$ (O), and $1.01\ a_0$ (H). For the full cluster including the $Si_6O_{18}H_6$ cap, the outer sphere is centered at $z=0.5431a_0$ with respect to Si', with radius $13.2227a_0$: in the calculation without the cap, the outer sphere is centered at $-3.0334a_0$ and has radius $12.1043a_0$. The α values used are the atomic α_{HF} from the tabulation of Schwarz,[73] with the exception of H, for which the spin-polarized value is used.[74] α for the intersphere and outer sphere regions are valence-electron weighted averages over the atoms in the cluster. The basis set includes angular functions up to $l=4$ on the outer sphere, $l=2$ on all Si, $l=1$ on O, and $l=0$ on H. This constitutes a polarization basis on Si (Si_d orbitals included) and is a minimum angular basis on O and H. The MS $X\alpha$ minimum angular basis has much more flexibility than a standard linear combination of atomic orbitals (LCAO) minimum basis set because the radial functions are not fixed before the calculation but are computed self-consistently by numerical integration. Only the angular flexibility of the atomic functions is restricted. Polarization based on O and H were not considered necessary here. Our primary interest is in the characteristics of the electronic structure of the defect, which is comparatively localized, and this is not greatly affected by the small amount of charge that would be accommodated in O_d or H_p functions in the silica phase and at the surface of the cluster.

III. RESULTS AND DISCUSSION

A. Defect orbital and spin populations

Our calculated values for the defect orbital atomic populations and the net atomic spin populations are reported in Table II. A number of important features of the P_b center are evident in these results. Most of the defect orbital (60%) is located on Si'. The delocalization away from the trivalent atom is limited in extent and highly directional. More than 93% of ϕ_d^α is concentrated on Si', its three nearest neighbors Si_{s1}, and the three Si_{b2} second-nearest neighbors which lie below Si_{s1} in the bulk *c*-Si. A contour plot showing the bonding structure in the defect orbital is presented in Fig. 3. It is effectively Si'-Si_{s1} nonbonding to antibonding (the negative lobe of the Si_{s1} 3*p* orbital is directed just above the node of Si' 3*p*, pointing at the positive lobe of that orbital) and is Si_{s1}—Si_{b2} bonding. Very little of ϕ_d^α delocalizes along the (111) surface onto the six Si_{s2} second-nearest neighbors or into more distant regions of the cluster.

In the largest cluster in particular, only 2.1% of ϕ_d^α is located in the SiO_2 phase and most of that (1.44%) resides on the three O_- atoms, due to direct overlap with the part of the Si' hybrid orbital which projects into the silica cavity. The net spin density likewise has small values in the SiO_2 half of the cluster. This is very plausi-

TABLE II. P_b model defect orbital populations and net spin populations.

	Defect orbital populations (%)[a]			Net spin populations (%)[b]		
	Unrelaxed $Si_{22}H_{21}/Si_6O_{18}H_6$	Unrelaxed $Si_{22}H_{27}$	Relaxed $Si_{22}H_{27}$	Unrelaxed $Si_{22}H_{21}/Si_6O_{18}H_6$	Unrelaxed $Si_{22}H_{27}$	Relaxed $Si_{22}H_{27}$
Si'	60.05	61.02	61.69	73.98	72.18	72.66
s	3.64	3.80	3.04	6.08	6.47	5.58
p	56.00	56.70	58.03	67.28	65.02	66.20
d	0.41	0.52	0.63	0.63	0.69	0.88
Si_{s1}	6.21	6.81	6.35	5.40	5.72	5.52
s	0.27	0.32	0.28	0.08	0.16	0.09
p	3.88	4.18	3.33	2.95	3.03	2.41
d	2.06	2.31	2.74	2.37	2.52	3.02
Si_{b2}	4.75	4.61	4.76	4.02	4.23	4.56
s	0.37	0.35	0.41	0.33	0.35	0.39
p	3.68	3.45	3.47	3.09	3.13	3.34
d	0.70	0.82	0.88	0.60	0.74	0.83
Si_{s2}	0.11	0.11	0.15	−0.18	−0.33	−0.43
Si_{b3}	0.24	0.21	0.19	−0.64	−0.37	−0.30
Si_{s3}	0.11	0.05	0.05	0.11	−0.18	−0.42
Si_{b4}	0.06	0.04	0.04	0.01	−0.25	−0.19
O_l	0.04			−0.08		
Si_r	0.03			0.00		
O_+	0.02			−0.25		
O_-	0.48			0.32		
O_t	0.03			−0.28		

[a]Percentages of the ϕ_d^α charge assigned to each site by the MS $X\alpha$ charge-partitioning procedure. The intersphere and outer sphere charges have both been partitioned onto the atomic centers.

[b]Sum over all occupied levels of the majority- minus minority-spin partitioned charge populations.

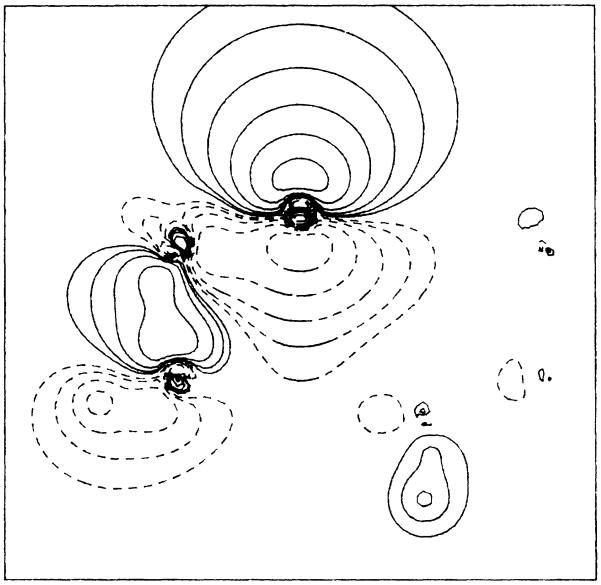

FIG. 3. Contour plot of the defect orbital in the relaxed $Si_{22}H_{27}$ model. The plot is in the xz plane and the y axis points into the page (same orientation as Fig. 1). The dimensions are $20a_0 \times 20a_0$. Si′ is the nucleus at top center, while Si_{b2} lies below Si_{s1} on the left. Contours begin at 0.2 and decrease by factors of 2. Positive and negative phases are represented by solid and dashed lines, respectively. The contours have been smoothed by mixing the atomic and intersphere representations of the wave function within each atomic sphere using a sigmoidal radial switching function.

ble behavior in view of the relative conductivities and dielectric constants of silicon and silica: We should not expect that an unpaired c-Si electron located at the interface would delocalize much into the SiO_2 phase, or that it would be able to polarize the silica significantly. The results in Table II illustrate this clearly. Because of the very small amount of ϕ_d^α amplitude and spin density in the silica cap and the Si_{s2} atoms bonded to it, the presence of the cap has only a small effect on the hyperfine interactions. The silica phase does significantly perturb other aspects of the electronic structure, which will be discussed in a future publication, and its presence prevents the c-Si interface from reconstructing away from a uniform (111) surface. But in the absence of reconstructions, the spin-dependent properties are not strongly affected. Because of this insensitivity to the cap, our relaxed-Si′ calculation has been carried out on the smaller $Si_{22}H_{27}$ cluster in which the cap is removed.

Our calculated values of defect orbital populations on Si′ are appreciably smaller than the values that have previously been suggested using the local-hybrid picture and isolated-atom values of $|\psi_{3s}(0)|^2$ and $\langle r^{-3}\rangle_{3p}$ for silicon.[18] Brower estimated that 80% of the defect orbital was localized on Si′: 9.6% s and 70.4% p. In the relaxed $Si_{22}H_{27}$ cluster we find only 62% of ϕ_d^α on Si′, divided as 3.0% s, 58.0% p, and 0.6% d. Much of the reason for this discrepancy is that the local-hybrid picture cannot consider polarization effects. We can see by comparing the defect orbital populations with net spin populations in Table II how important a role interatomic spin polarization plays in the P_b center. The spin population on Si′ is significantly greater than would be expected from the ϕ_d^α charge distribution because charge in the filled valence levels is free to polarize so as to concentrate extra majority-spin density on Si′, where it is stabilized by exchange interactions. In the net spin distribution the localization on Si′ is increased from 62% to 73% (5.6% s, 66.2% p, 0.9% d). The local-hybrid estimate is a somewhat more accurate gauge of the net spin populations than of the defect orbital itself.

B. Hyperfine interactions

In the present study we do not use the spin populations of Table II in conjunction with semiempirical formulas and assumed atomic integrals to estimate hyperfine couplings. Instead we calculate the hyperfine tensors directly from our all-electron self-consistent wave function. The phenomenological spin Hamiltonian which expresses the interaction of a paramagnetic system like the neutral P_b center with an external magnetic field $\mathbf{H}$ can be written,

$$\hat{H} = \mu_B \mathbf{H}\cdot\vec{\mathbf{g}}\cdot\mathbf{S} + \sum_N \hat{H}_N^{\mathrm{hf}} , \tag{1}$$

where μ_B is the Bohr magneton. The electron spin couples to the applied field through the g tensor, and couples to each nearby nucleus N having a nonzero magnetic dipole moment through a hyperfine Hamiltonian $\hat{H}_N^{\mathrm{hf}}$. The individual hyperfine interactions each separate into an isotropic Fermi contact-interaction term and a traceless dipolar part:

$$\hat{H}_N^{\mathrm{hf}} = \hat{H}_N^{\mathrm{iso}} + \hat{H}_N^{\mathrm{dip}} \tag{2a}$$

$$= a^N \mathbf{I}_N\cdot\mathbf{S} + \mathbf{I}_N\cdot\vec{\mathbf{A}}^N\cdot\mathbf{S} \tag{2b}$$

Additional second-order terms $\hat{H}_N^{\mathrm{SO}}$ which depend on interactions of the ground state with excited states through spin-orbit coupling can also contribute to the hyperfine Hamiltonian.[24,25] In heavy atoms of the first transition row and beyond, these contributions can be very large: since their calculation depends on a knowledge of the excited states and excitation energies of the system they are rarely computed directly from a wave function but are estimated using ligand-field theory approximations and empirical or isolated-atom values of coupling constants, orbital moments, and excitation energies.[75] Fortunately these second-order terms are negligible for the P_b center. Approximate relations which exist between the experimental g tensor and the orbital hyperfine tensor[24,25,55] indicate that the contribution of second-order terms is no greater than ~ 0.5 G, and this can safely be neglected.

The isotropic and dipole-dipole terms in Eq. (2b) can be computed from the ground-state wave function alone. The MS $X\alpha$ wave function for the P_b center is a spin-polarized, single-determinant $M_S = \frac{1}{2}$ wave function constructed from molecular spin-orbitals $\phi_\mu^{\alpha,\beta}$. Neglecting spin contamination, which should be small in this system,

$$a^N=\frac{8\pi}{3}g_e\mu_B g_N\mu_n\left[\sum_{\mu}^{\text{occ}}\langle\phi_\mu^\alpha|\delta^3(\mathbf{r}_N)|\phi_\mu^\alpha\rangle-\sum_{\mu}^{\text{occ}}\langle\phi_\mu^\beta|\delta^3(\mathbf{r}_N)|\phi_\mu^\beta\rangle\right] \quad (3)$$

$$A_{ij}^N=g_e\mu_B g_N\mu_n\times\left[\sum_{\mu}^{\text{occ}}\left\langle\phi_\mu^\alpha\left|\frac{3r_{Ni}r_{Nj}-\delta_{ij}r_N^2}{r_N^5}\right|\phi_\mu^\alpha\right\rangle-\sum_{\mu}^{\text{occ}}\left\langle\phi_\mu^\beta\left|\frac{3r_{Ni}r_{Nj}-\delta_{ij}r_N^2}{r_N^5}\right|\phi_\mu^\beta\right\rangle\right], \quad (4)$$

where g_N is the nuclear magnetogyric ratio with $g_N=\mu_N/I_N$, μ_N is the magnetic moment of nucleus N, μ_n is the nuclear magneton, and g_e is the free-electron g value. The subscripts N on the radius vectors in Eqs. (3) and (4) indicate that nucleus N is to be taken as the origin of electronic coordinates in the matrix elements.

The terms in large parentheses in Eq. (3) represent the electron spin density at the nucleus (net minority-spin minus minority-spin density in units of electrons/a_0^3). In a spin-restricted model the α and β spin contributions from all the doubly filled orbitals cancel and only a single term remains in the summations, representing the amplitude at nucleus N due to the singly occupied defect level ϕ_d^α. However, in a spin-polarized picture ϕ_μ^α and ϕ_μ^β are allowed to have different spatial forms so that in the general case every orbital μ not constrained by symmetry to vanish at nucleus N will make some nonzero contribution. Similar considerations apply to the contributions to anisotropic hyperfine coupling in Eq. (4), where the operator is the electric field gradient.

The theoretical hyperfine tensors in our P_b center cluster models are reported in Table III along with recent experimental results from ESR spectra. The primary isotropic hyperfine interaction is located, as we should expect, on the defect atom Si′ where the bulk of the spin density is concentrated. The negative sign of $a^{\text{Si}'}$ indicates net majority-spin density at the nucleus, because $g_{^{29}\text{Si}}$ is negative [cf. Eq. (3)]. The sign of the coupling constant is not measured by ESR experiments, but the negative sign we find here is almost certainly correct. In high-spin transition metals, very strong core polarizations can exist which can induce a net minority-spin density at the nucleus of atoms which carry predominantly majority spin in the valence shell.[56,75] But to our knowledge, core polarizations are never strong enough in atoms of the second row to cause such a reversal in sign.

In Table IV we give a breakdown of the isotropic hyperfine coupling at the most important nuclei in the relaxed $Si_{22}H_{27}$ cluster according to contributions from the direct versus induced interactions. There is a net isotropic hyperfine interaction at Si′ of -128.6 G in this cluster. Only -80.1 G of this is due to the direct contribution from the defect orbital ϕ_d^α itself; polarization of the doubly-occupied valence orbitals contributes an additional -65.8 G, while core polarization produces opposing effects which are smaller, but still significant ($+4.5$ G from the Si'_{2s} levels, and $+12.7$ G from the Si'_{1s} core). The large size of the valence polarization illustrates again the difficulty in working backwards from experimental hyperfine couplings within the local-hybrid model to derive defect orbital populations. Other differences from the local-hybrid estimate are created by variations in the self-consistent field (SCF) values of matrix elements appearing in Eqs. (3) and (4) as compared to the fixed, isolated-atom values of $|\psi_{3s}(0)|^2$ and $\langle r^{-3}\rangle_{3p}$ used in the simple picture. The defect orbital and each of the valence levels have slightly different values of the matrix elements, reflecting perturbations in the shape of atomic orbitals in the molecular environment. The qualitative predictions of the local-hybrid model are largely correct and its simplicity makes it a valuable interpretative tool, but it is not very reliable for quantitative prediction of the defect orbital distribution at second-row atoms.

The anisotropic hyperfine tensor at Si′ is axial, as required by the C_{3v} symmetry of the system. The principal component points along the z axis ($\langle 111\rangle$ direction) and has the same negative sign as the isotropic coupling (Table III). The negative sign of $A_{zz}^{\text{Si}'}$ is to be expected from the prolate majority-spin distribution of the p_z-like defect orbital about Si′. This is also consistent with the experimental finding that the hyperfine splitting is greatest when the applied field points in the $\langle 111\rangle$ direction, giving an effective splitting of $a+A_{zz}$ G, and is smallest when the field is normal to that direction, for an effective splitting of $a-\frac{1}{2}A_{zz}$ G.

In Table II we saw that the defect orbital charges and net spin populations on the atoms of the silica cap are small in the $Si_{22}H_{21}/Si_6O_{18}H_6$ cluster. This results in only small differences between the hyperfine interactions of the clusters with and without the SiO_2 capping ring in the first two columns of Table III. These unrelaxed clusters produce hyperfine couplings at Si′ which are too large compared to experiment. This is what we should anticipate. We know that as Si′ relaxes downward toward the plane of its nearest neighbors Si_{s1}, the Si′ s character of ϕ_d^α will be diminished and the isotropic hyperfine coupling will decrease. When Si′ is frozen at the tetrahedral position the computed hyperfine coupling ought to be too large.

Using the relaxed value of $\Delta z_{\text{Si}'}$, our calculated $a^{\text{Si}'}$ is reduced from -152.7 to -128.6 G. The principal anisotropic component $A_{zz}^{\text{Si}'}$ is not greatly affected by the relaxation (-57.8 to -59.2 G). The relaxed values are in very good agreement with experiment: closer agreement than this would be fortuitous, given the uncertainty in $\Delta z_{\text{Si}'}$ and the muffin-tin approximations inherent in the MS $X\alpha$ method.

C. Superhyperfine interactions

The good agreement of our Si′ hyperfine results with experiment suggests that these calculations should also be useful in assigning the superhyperfine interaction first observed by Brower[18] in his ESR study of the P_b center. With the magnetic field oriented normal to the (111) surface (along the z axis) a small superhyperfine shoulder of ~ 15 G was found in the wings of the central line of the

ESR spectrum. It is very important in understanding the structure of a defect center like the P_b center to be able to identify the source of such superhyperfine interactions correctly, and to understand them in terms of the local electronic structure. Just as the primary hyperfine interaction gives specific information about the nature of the defect atom and its hybridization and reconstruction, the superhyperfine tensors reflect more extended interactions between the defect atom and its host lattice. This extra information about the response of the host can be valuable for distinguishing among alternate possibilities for the setting of the defect in the solid-state matrix, and for interpreting the defect-host interaction in simple chemical terms.

In the absence of a detailed picture of the bonding in the P_b center it would be natural to assume that the delocalization of spin population away from Si′ would be greatest onto the nearest neighbors Si_{s1} and progressively smaller on second- or third-nearest neighbors, as if the spin were extending into a uniform continuum. It would likewise be natural to expect that the superhyperfine interactions should decrease monotonically and isotropically with distance from Si′. Tables II and III show that these are not, however, good assumptions for the P_b center. The delocalization of spin population is indeed greatest onto Si_{s1}, as expected (5.5% per Si_{s1}) but the delocalization onto second-nearest neighbors is highly anisotropic (4.6% on each of the three Si_{b2}, but −0.43% on the six Si_{s2}).

The most striking contradiction to naive expectations

TABLE III. Model P_b center hyperfine tensors (G). Calculated values of a are converted to units of G using $a\,(\mathrm{G}) = 285.522 g_N \langle \delta^3(\mathbf{r}_N) \rangle_{\alpha\text{-}\beta}$ (a.u.) for nucleus N: $g_{^{29}\mathrm{Si}} = -1.11052$, $g_{^{17}\mathrm{O}} = -0.75748$ (Ref. 76). The conversion factor for the anisotropic A tensor is smaller by a factor of $8\pi/3$. The principal axes of A coincide with local coordinate axes only for Si′. For other atoms the principal component of A is labeled by the coordinate axis with which it makes the smallest angle (primed subscripts). The asymmetry parameter $\eta = (A_{11} - A_{22})/A_{33}$, where A_{ii} labels the principal values in order of increasing magnitude. θ is the counterclockwise rotation angle about the axis out of the paper in Fig. 1 (the $-Y$ axis) required to bring the coordinate axes into coincidence with the principal axes of A. See Fig. 4 for illustrations.

		Unrelaxed $Si_{22}H_{21}/S_6O_{18}H_6$	Unrelaxed $Si_{22}H_{27}$	Relaxed $Si_{22}H_{27}$	Expt.[a]	Expt.[b]
Si′	a	−151.94	−152.73	−128.62	113±7[c]	106[c]
	A_{zz}	−65.57	−57.76	−59.16	44±13	45
Si_{s1}	a	0.45	−0.17	1.24		
	$A_{x'x'}$	−2.33	−2.38	−1.64		
	η	0.19	0.08	0.09		
	θ	42.1°	33.2°	33.6°		
Si_{b2}	a	−9.67	−8.31	−9.84	15[c,d]	13.3[c]
	$A_{z'z'}$	−3.36	−3.04	−3.12		1.9
	η	0.03	0.03	0.03		
	θ	−3.5°	−2.3°	−1.6°		∼0°
Si_{s2}	a	1.68	2.24	1.91		
	$A_{y'y'}$	0.23	0.25	0.22		
	η	0.36	0.23	0.30		
Si_{b3}	a	2.19	2.73	2.82		
	$A_{y'y'}$	0.18	0.15	0.15		
	η	0.74	0.62	0.52		
Si_{s3}	a	0.38	0.94	0.99		
	$A_{x'x'}$	−0.13	−0.11	−0.11		
	η	0.04	0.05	0.08		
Si_{b4}	a	0.56	1.20	1.24		
	$A_{x'x'}$	−0.10	−0.10	−0.10		
	η	0.01	0.50	0.51		
Si_r	a	−0.24				
	$A_{x'x'}$	−0.12				
	η	0.30				
O_-	a	−2.25				
	$A_{z'z'}$	−0.68				
	η	0.11				
	θ	38.8°				

[a]Reference 18.

[b]Reference 84.

[c]The sign of the hyperfine interaction is not measured by the ESR experiment: the experimental couplings represent absolute values.

[d]Estimated from the figure in Ref. 18, with the field along the ⟨111⟩ direction.

TABLE IV. Direct and induced contributions to isotropic hyperfine coupling constants in the relaxed $Si_{22}H_{27}$ P_b model cluster (G).

	Si′	Si_{s1}	Si_{b2}
Defect orbital	−80.05	−7.22	−10.33
Valence polarization	−65.81	7.81	−0.35
2s core polarization	4.53	0.41	0.32
1s core polarization	12.71	0.24	0.51
Net	−128.62	1.24	−9.84

is that despite the significant spin population on the nearest neighbors Si_{s1}, only a small isotropic hyperfine coupling is produced on them; and in the relaxed cluster that coupling has the minority-spin sign, not the majority-spin sign (+1.2 G). The principal anisotropic component $A_{x'x'}^{Si_{s1}}$ is only −1.6 G, and it is not possible for this tensor to be responsible for the 15-G shoulder regardless of the orientation of the applied field. It is actually the three second-nearest neighbors Si_{b2} which produce the superhyperfine shoulder. Both the size and the orientation of this calculated Si_{b2} tensor are consistent with the experimental shoulder seen by Brower.[18] The isotropic coupling $a^{Si_{b2}}$ is calculated to be −9.8 G: when the field is in the z direction (Table III), this is reinforced by the principal component of the dipolar tensor $\overleftrightarrow{A}$ (−3.1 G), giving a net interaction of −13 G, close to the experimentally observed splitting. The identification of Si_{b2} with this shoulder is straightforward from our calculations, because no other interaction in the cluster is close to the correct size. The characteristic error in hyperfine matrix elements calculated by the MS $X\alpha$ method is ~20–30 % at most in a system of this sort: the errors in our Si′ couplings in Table III, for example, are in line with previous experience. If there were another interaction in the cluster of about 8–15 G, it would require extra information to distinguish between them. But all atoms in the cluster apart from Si_{b2} are calculated to have much smaller hyperfine couplings (<3 G), too small by a factor of 3 or 4 to account for the observed shoulder. This discrepancy is too large to be an artifact of our calculational methods.

It should be noted that experimental intensity ratios in ESR spectra, which are often very useful in identifying the source of an interaction, would not distinguish between Si_{s1} and Si_{b2}. In both cases three atoms are involved. Without specific bonding information we might have imagined that a second-neighbor coupling would necessarily have an intensity ratio of 9; but the second neighbors are not all required by symmetry to be equivalent, and in this case the couplings at the two symmetry-equivalent sets Si_{b2} and Si_{s2} differ by a wide margin.

The small minority-spin coupling at Si_{s1} is not an isolated or anomalous result, but is consistent with well-understood spin polarization effects. It can be simply explained in the context of small-molecule chemistry. The lobe structure of the local atomic orbitals in the Si′—$(Si_{s1})_3$ system is very similar to that of SiH_3, with the H_{1s} atomic orbitals replaced by a hybrid on each Si_{s1} directed at the Si′ atom.[70] It should therefore show many of the same trends as silyl radical and other AH_3 radicals as a function of geometry variation.

When the heavy atom in an AH_3 radical occupies the same plane as the H atoms so that the whole molecule is planar, the defect orbital ϕ_d^α becomes purely p-like. The σ-π separability of this planar system prevents any mixing of the H_{1s} orbitals into ϕ_d^α, so that majority-spin density is prohibited by symmetry from delocalizing onto the hydrogens. However, a sizable minority spin density can be induced at the protons by polarization effects. Among the filled valence orbitals, the majority-spin levels ϕ_μ^α will tend to concentrate more of their amplitude on the central atom A to benefit from the exchange stabilization there. Their minority-spin partners ϕ_μ^β are oppositely polarized. The net result is a minority-spin coupling at the protons. This is characteristic of planar AH_3 systems; the same behavior is seen at the in-plane H atoms of planar organic π radicals.[22,77]

In pyramidal AH_3 radicals, on the other hand, the σ-π separability breaks down. If we imagine raising the central atom up out of the nearest-neighbor plane, the polarization effects continue to operate but positive spin density is gradually built in at the nearest-neighbor position by direct overlap: the net spin density at the nucleus can pass through zero and become positive. For silicon, which has a negative value of $g_{^{29}Si}$, this corresponds to $a>0$ on Si_{s1} in the planar geometry, $a<0$ for highly pyramidal conformations. For a range of values of $\Delta z_{Si'}$ corresponding to moderately pyramidal radicals, the nearest-neighbor isotropic hyperfine coupling is small. This near-cancellation of opposing effects has resulted, for example, in a long controversy in the literature over the correct sign of the proton coupling constant in the SiH_3 radical itself.[78–83]

The situation in the P_b center is somewhat more complicated than in silyl radical because of the presence of polarizable cores and the possibility of rehybridization and hyperconjugative effects at Si_{s1} as a function of bond angle. But we can see by comparing unrelaxed and relaxed $Si_{22}H_{27}$ results in Table III that the net trend is the same as expected from the analogy with SiH_3. As the geometry at Si′ becomes more nearly planar, the isotropic hyperfine coupling at Si_{s1} goes from slightly negative to slightly positive. Table IV exhibits the opposing effects explicitly. The direct majority-spin contribution from ϕ_d^α at Si_{s1} is −7.22 G; but this is counterbalanced by the induced contribution of +7.81 G due to valence polarization.

At the time our calculations were completed, the only experimental superhyperfine result available for the P_b center was the 15-G shoulder observed by Brower with the field in the ⟨111⟩ direction.[18] Subsequently, Carlos examined this signal in SIMOX materials[84] (last column of Table III). In that study, the isotropic and principal anisotropic components were determined to have magnitudes of 13.3 and 1.9 G, respectively: our calculated values of −9.84 and −3.12 G agree satisfactorily with those results.

Most importantly, Carlos found the principal com-

ponent of the anisotropic tensor to be directed within a few degrees of the ⟨111⟩ axis. Figure 4 illustrates the significance of that result. The calculated isotropic hyperfine coupling at each atom in the figure is given inside a sphere surrounding the nucleus, while the principal anisotropic components are attached to the axes which diagonalize the tensor. When an unpaired electron occupies a localized site, the principal component of the anisotropic tensor on its nearest neighbors tends to point at the position of the electron, as $A_{x'x'}^{Si_{s1}}$ in the figure points just above Si′ at the hybrid orbital. But since the field gradient operator in Eq. (4) falls off rapidly as a function of distance, the tensors of more distant atoms have a greater tendency to point along bond directions at any of their own neighbors which carry a significant amount of spin. This is the case for $A_{z'z'}^{Si_{b2}}$ in Fig. 4. These simple considerations imply that, whatever the particular values of the components, the superhyperfine tensor on Si_{s1} should be tilted strongly away from the ⟨111⟩ direction while the Si_{b2} tensor would be much more closely aligned with that axis. The direction of the experimental tensor is therefore in itself a significant indication that the observed splitting should be associated with Si_{b2} rather than Si_{s1}, even apart from the evidence of our theoretical calculations.

There are still several important points to be resolved experimentally. We find the isotropic and anisotropic interactions on Si_{b2} to have the negative sign, and this has not been tested by the ESR experiments which have been done. We also find the Si_{b2} tensor to be nearly axial; the asymmetry parameter η is only 0.03. This nearly axial character is not required by symmetry, and it would be very interesting to know if this is correct experimentally. Both these points could in principle be determined by multiple-resonance experiments such as electron-nuclear double resonance (ENDOR).

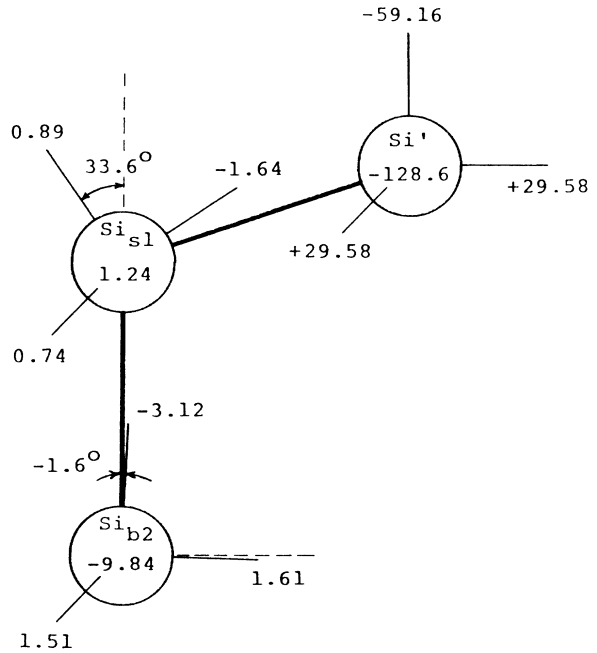

FIG. 4. Hyperfine tensors of the atoms with appreciable amplitude in the defect orbital. Relaxed $Si_{22}H_{27}$ model. Orientation as in Figs. 1 and 3.

IV. CONCLUSIONS

Spin-polarized MS $X\alpha$ calculations have been carried out on large cluster models of the P_b center at the Si(111)/SiO_2 interface. We find that the silica phase can be modeled by a single ditrigonal ring of six SiO_4 tetrahedra, bonded to the hexagon of Si_{s2} atoms surrounding the defect atom at the (111) surface. The ditrigonal ring is common in naturally occurring phases of silica, particularly in tridymites. This model of the SiO_2 phase introduces no abnormal strains in either phase or at the interface, and it provides a microvoid above the defect atom of the appropriate size to allow Si′ to be passivated by an H atom diffusing through the silica.

We find that the delocalization of the defect orbital and the distribution of spin density in the P_b center are limited in extent and very anisotropic. The only atoms which carry significant spin populations are Si′, its three nearest neighbors Si_{s1}, and the three Si_{b2} second-nearest neighbors below Si′ in the bulk silicon. Because of the very small degree of spin delocalization into the silica phase, it makes little difference to the calculated hyperfine tensors whether the SiO_2 cap is present or not.

The hyperfine tensor at Si′ is modeled very well by our relaxed-cluster calculation, using a relaxation $\Delta z_{Si'}$ at the defect atom close to the average from recent semiempirical and *ab initio* calculations. Spin-polarization effects are found to be important in the P_b center in several ways. The defect orbital is less concentrated on Si′ than the local-hybrid model would predict because polarization effects bring additional spin onto Si′. The hybrid-orbital picture gives a somewhat better description of the net spin populations than of the unpaired spin-orbital itself. The hyperfine coupling at the three nearest neighbors Si_{s1} is found to be small in the P_b center because of the opposing effects of direct spin delocalization and induced exchange polarization. This can be understood by a straightforward analogy with the behavior of simple AH_3 radicals as a function of H—A—H bond angle.

The largest superhyperfine interaction in the cluster is actually located at the three second-nearest neighbors Si_{b2}. The magnitudes of the isotropic and principal anisotropic components and the orientation of the tensor that we predict at Si_{b2} agree well with experimental ESR studies of the superhyperfine interaction carried out subsequent to the completion of the present theoretical work. The good agreement of our theoretical hyperfine and superhyperfine tensors with experiment gives strong support to the standard threefold-coordinated model of the P_b center in which the defect orbital points into a small microvoid in the silica phase.

The present study illustrates both the strengths and the limitations of the widely used local-hybrid picture. That picture has been a very valuable tool for interpreting ESR spectra of localized paramagnetic defects. It constructs a qualitatively correct model for the spin localization and hybridization of the defect atom, and this can be effective in giving an overall picture of the defect. Our calcula-

tions confirm, after all, a basic structural model of the P_b center which was first proposed using a local-hybrid picture alone. But this picture is less successful in treating the smaller hyperfine couplings which might be associated with a defect. It is very unlikely, for example, that the identification of the P_b superhyperfine interaction with Si_{b2} rather than Si_{s1} would have been made within a local-hybrid framework. This is not an isolated case. The small superhyperfine interactions are particularly sensitive to polarization and other second-order effects because their couplings are not necessarily dominated by a large direct majority-spin contribution. However, it is essential to assign these smaller couplings to the correct atoms and to give a physically reasonable rationale for their signs and magnitudes in order to arrive at a consistent, complete picture of the interactions between the defect and its host lattice.

Self-consistent spin-polarized calculations which treat the cores as well as the valence levels explicitly do include all the physical interactions which are important for producing hyperfine couplings in systems composed of first- and second-row atoms. The present work has shown that the spin-polarized MS $X\alpha$ method can be applied successfully to both the large and small couplings of the P_b center. We expect it to be equally useful in the study of other paramagnetic defects in the solid state, particularly in assigning the smaller interactions and resolving ambiguities among alternate proposed structures. Other such systems are currently under study.

ACKNOWLEDGMENTS

We thank Dave Griscom, Art Edwards, and Bill Carlos for many stimulating and helpful discussions of the structure of defect centers in Si/SiO_2 systems. One of us (M.C.) is grateful to the National Research Council for support during the completion of the theoretical calculations reported here, and to the U.S. Office of Naval Technology for current support. This research was supported by the Office of Naval Research (ONR), U.S. Department of Defense.

[1]B. E. Deal, J. Electrochem. Soc. **121**, 198C (1974).
[2]P. Balk and N. Klein, Thin Solid Films **89**, 329 (1982).
[3]P. M. Lenahan and P. V. Dressendorfer, J. Appl. Phys. **54**, 1457 (1983).
[4]P. M. Lenahan and P. V. Dressendorfer, J. Appl. Phys. **55**, 3495 (1984).
[5]E. H. Poindexter, G. J. Gerardi, M.-E. Rueckel, P. J. Caplan, N. M. Johnson, and D. K. Biegelsen, J. Appl. Phys. **56**, 2844 (1984).
[6]P. M. Lenahan, K. L. Brower, P. V. Dressendorfer, and W. C. Johnson, IEEE Trans. Nucl. Sci. **NS-28**, 4105 (1981).
[7]S. K. Lai, Appl. Phys. Lett. **39**, 58 (1981).
[8]M. V. Fischetti, R. Gastaldi, F. Maggioni, and A. Modelli, J. Appl. Phys. **53**, 3129 (1982).
[9]M. C. Chen and D. V. Lang, Phys. Rev. Lett. **51**, 427 (1983).
[10]N. M. Johnson, D. K. Biegelsen, M. D. Moyer, S. T. Chang, E. H. Poindexter, and P. J. Caplan, Appl. Phys. Lett. **43**, 563 (1983).
[11]B. Henderson, Appl. Phys. Lett. **44**, 228 (1984).
[12]W. B. Jackson, N. M. Johnson, and D. K. Biegelsen, Appl. Phys. Lett. **43**, 195 (1983).
[13]C. H. Seager and P. M. Lenahan, J. Appl. Phys. **58**, 2709 (1985).
[14]Y. Nishi, Jpn. J. Appl. Phys. **10**, 52 (1971).
[15]P. J. Caplan, E. H. Poindexter, B. E. Deal, and R. R. Razouk, J. Appl. Phys. **50**, 5847 (1979).
[16]C. Brunström and C. Svensson, Solid State Commun. **37**, 399 (1981).
[17]E. H. Poindexter, P. J. Caplan, B. E. Deal, and R. R. Razouk, J. Appl. Phys. **52**, 379 (1981).
[18]K. L. Brower, Appl. Phys. Lett. **43**, 1111 (1983).
[19]A. Stesmans, J. Braet, J. Witters, and R. F. Dekeersmaecker, Surf. Sci. **141**, 255 (1984).
[20]D. L. Griscom, J. Appl. Phys. **58**, 2524 (1985).
[21]G. D. Watkins and J. W. Corbett, Phys. Rev. **134**, A1359 (1964).
[22]J. R. Morton, Chem. Rev. **64**, 453 (1964).
[23]C. J. Ballhausen, *Introduction to Ligand Field Theory* (McGraw-Hill, New York, 1962).
[24]C. P. Keijzers and E. de Boer, J. Chem. Phys. **57**, 1277 (1972).
[25]C. P. Keijzers and E. de Boer, Mol. Phys. **29**, 1007 (1975).
[26]F. J. Feigl, W. B. Fowler, and K. L. Yip, Solid State Commun. **14**, 225 (1974).
[27]D. A. Case and M. Karplus, J. Am. Chem. Soc. **99**, 6182 (1977).
[28]T. Sakurai and T. Sugano, J. Appl. Phys. **52**, 2889 (1981).
[29]K. L. Ngai and C. T. White, J. Appl. Phys. **52**, 320 (1981).
[30]A. S. Carrico, R. J. Elliott, and R. A. Barrio, Phys. Rev. B **34**, 872 (1986).
[31]Y. Bar-Yam and J. D. Joannopoulos, Phys. Rev. Lett. **56**, 2203 (1986).
[32]K. L. Yip and W. B. Fowler, Phys. Rev. B **11**, 2327 (1975).
[33]A. H. Edwards and W. B. Fowler, J. Phys. Chem. Solids **46**, 841 (1985).
[34]A. H. Edwards, J. Electron. Mater. **14a**, 491 (1985).
[35]A. H. Edwards, Phys. Rev. B **36**, 9638 (1987).
[36]R. C. Bingham, M. J. S. Dewar, and D. H. Lo, J. Am. Chem. Soc. **97**, 1285 (1975).
[37]P. Bischof, J. Am. Chem. Soc. **98**, 6844 (1976).
[38]M. J. S. Dewar and W. Thiel, J. Am. Chem. Soc. **99**, 4899 (1977).
[39]L. C. Synder and Z. Wassermann, Surf. Sci. **77**, 52 (1978).
[40]A. Redondo, W. A. Goddard III, T. C. McGill, and G. T. Surratt, Sol. St. Comm. **20**, 733 (1976).
[41]J. C. Slater, *The Self-Consistent Field for Molecules and Solids: Quantum Theory of Molecules and Solids Volume 4* (McGraw-Hill, New York, 1974).
[42]D. A. Case, Annu. Rev. Phys. Chem. **33**, 151 (1982).
[43]M. Cook and D. A. Case, XASW: A FORTRAN Program Package for Atomic $X\alpha$ and Molecular Multiple-Scattering $X\alpha$ Electronic Structure Calculations, Quantum Chemistry Program Exchange No. 465, Bloomington, IN 47405.
[44]B. Cartling, B. Roos, and U. Wahlgren, Chem. Phys. Lett. **21**, 380 (1973).
[45]L. A. Hemstreet, Phys. Rev. B **15**, 834 (1977).
[46]J. A. Tossell, D. J. Vaughan, and K. H. Johnson, Chem. Phys.

Lett. **20**, 329 (1973).
[47]K. H. Johnson, H. J. Kolari, J. P. de Neufville, and D. L. Morel, Phys. Rev. B **21**, 643 (1980).
[48]M. E. Eberhart, K. H. Johnson, and D. Adler, Phys. Rev. B **26**, 3138 (1982).
[49]I. P. Batra and S. Ciraci, Phys. Rev. Lett. **34**, 1337 (1975).
[50]I. P. Batra and S. Ciraci, Phys. Rev. Lett. **36**, 170 (1976).
[51]C. T. White, F. W. Kutzler, and M. Cook, Phys. Rev. Lett. **56**, 252 (1986).
[52]M. Cook and M. Karplus, J. Chem. Phys. **72**, 7 (1980).
[53]D. A. Case, M. Cook, and M. Karplus, J. Chem. Phys. **73**, 3294 (1980).
[54]M. Cook and M. Karplus, J. Am. Chem. Soc. **107**, 257 (1985).
[55]S. F. Sontum and D. A. Case, J. Phys. Chem. **86**, 1596 (1982).
[56]M. Cook and M. Karplus, J. Chem. Phys. **83**, 6344 (1985).
[57]M. Cook and C. T. White, Phys. Rev. Lett. **59**, 1741 (1987).
[58]W. Parrish, Acta Crystallogr. **13**, 838 (1960).
[59]D. R. J. Boyd, J. Chem. Phys. **23**, 922 (1955).
[60]W. H. Zachariasen and H. A. Plettinger, Acta Crystallogr. **18**, 710 (1965).
[61]W. S. Benedict, N. Gailar, and E. K. Plyler, J. Chem. Phys. **24**, 1139 (1956).
[62]W. H. Baur, Acta Crystallogr. Sect. B **36**, 2198 (1980).
[63]K. Kihara, Z. Kristallogr. **148**, 237 (1978).
[64]W. A. Dollase and W. H. Baur, Am. Mineral **61**, 971 (1976).
[65]J. H. Konnert, J. Karle, and G. A. Ferguson, Science **179**, 177 (1973).
[66]J. H. Konnert, P. d'Antonio, and J. Karle, J. Non-Cryst. Solids **53**, 135 (1982).
[67]A. Ourmazd, D. W. Taylor, J. A. Rentschler, and J. Bevk, Phys. Rev. Lett. **59**, 213 (1987).
[68]K. Kihara, Z. Kristallogr. **152**, 95 (1980).
[69]L. Pauling, *The Nature of the Chemical Bond,* 3rd ed. (Cornell University Press, Ithaca, NY, 1960), p. 260.
[70]T. A. Albright, J. K. Burdett, and M. H. Whangbo, *Orbital Interactions in Chemistry* (Wiley, New York, 1985), pp. 133–136, 140–145.
[71]D. Deaven, M. Cook, and C. T. White, unpublished MNDO, MOPN, and GAUSSIAN82 calculations.
[72]A. H. Edwards, Ref. 34; A. H. Edwards (private communication).
[73]K. Schwarz, Phys. Rev. B **5**, 2466 (1972).
[74]J. C. Slater, Int. J. Quantum Chem. Symp. **7**, 533 (1973).
[75]A. Abragam and B. Bleaney, *Electron Paramagnetic Resonance of Transition Ions* (Dover, New York, 1986).
[76]G. H. Fuller, J. Phys. Chem. Ref. Data **5**, 835 (1976).
[77]H. M. McConnell, J. Chem. Phys. **28**, 1188 (1958).
[78]R. L. Morehouse, J. J. Christiansen, and W. Gordy, J. Chem. Phys. **45**, 1751 (1966).
[79]S. W. Bennett, C. Eaborn, A. Hudson, R. A. Jackson, and K. D. K. Root, J. Chem. Soc. A **1970**, 348.
[80]I. Biddles and A. Hudson, Mol. Phys. **25**, 707 (1973).
[81]V. Barone, J. Douady, Y. Ellinger, R. Subra, and F. Pauzat, Chem. Phys. Lett. **65**, 542 (1979).
[82]Y. Ellinger, F. Pauzat, V. Barone, J. Douady, and R. Subra, J. Chem. Phys. **72**, 6390 (1980).
[83]K. Ohta, H. Nakatsuji, I. Maeda, and T. Yonezawa, Chem. Phys. **67**, 49 (1982).
[84]W. E. Carlos, Appl. Phys. Lett. **50**, 1450 (1987), and private communication.